Photoacoustics 33 (2023) 100551

Contents lists available at ScienceDirect

Photoacoustics

journal homepage: www.elsevier.com/locate/pacs

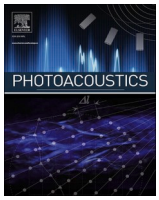

Quantification of prefrontal cortical neuronal ensembles following conditioned fear learning in a Fos-LacZ transgenic rat with photoacoustic imaging *in Vivo*

James I. Matchynski [a,b,c,d], Timothy S. Cilley [a], Nareen Sadik [a], Kassem M. Makki [c], Min Wu [c], Rayyan Manwar [e], Alexander R. Woznicki [c], Srinivasu Kallakuri [a], Cynthia L. Arfken [a,b], Bruce T. Hope [f], Kamran Avanaki [e], Alana C. Conti [a,b,c], Shane A. Perrine [a,b,*]

[a] *Department of Psychiatry and Behavioral Neurosciences, Wayne State University School of Medicine, Detroit, MI, USA*
[b] *Translational Neuroscience Program, Wayne State University School of Medicine, Detroit, MI, USA*
[c] *John D. Dingell Veterans Affairs Medical Center, Detroit, MI, USA*
[d] *Wayne State MD/PhD Program, Wayne State University School of Medicine, Detroit, MI, USA*
[e] *University of Illinois at Chicago, Department of Bioengineering, Chicago, IL, USA*
[f] *The National Institute on Drug Abuse (NIDA), Intramural Research Program, Baltimore, MD, USA*

ARTICLE INFO

Keywords:
Fos-LacZ transgenic rat
Neuronal ensembles
Photoacoustic imaging
Optoacoustic imaging
Functional imaging
Molecular imaging
Fear-conditioning
Medial prefrontal cortex

ABSTRACT

Understanding the neurobiology of complex behaviors requires measurement of activity in the discrete population of active neurons, neuronal ensembles, which control the behavior. Conventional neuroimaging techniques ineffectively measure neuronal ensemble activity in the brain *in vivo* because they assess the average regional neuronal activity instead of the specific activity of the neuronal ensemble that mediates the behavior. Our functional molecular photoacoustic tomography (FM-PAT) system allows direct imaging of Fos-dependent neuronal ensemble activation in Fos-LacZ transgenic rats in vivo. We tested four experimental conditions and found increased FM-PAT signal in prefrontal cortical areas in rats undergoing conditioned fear or novel context exposure. A parallel immunofluorescence ex vivo study of Fos expression found similar findings. These findings demonstrate the ability of FM-PAT to measure Fos-expressing neuronal ensembles directly *in vivo* and support a mechanistic role for the prefrontal cortex in higher-order processing of response to specific stimuli or environmental cues.

1. Introduction

Existing functional neuroimaging techniques, for example functional magnetic resonance imaging (fMRI), assess the average activity of neural cells in a given volume [1–4]. However, the majority of cells in this space do not contribute to the assessment of ongoing stimuli and related response behavior [5,6]. The learned behaviors are thought to be encoded and mediated by specific patterns of sparsely distributed neurons in the brain, known as neuronal ensembles, which correspond to the specific task or behavior elicited. Only a small proportion of neurons in a given brain area (*i.e.*, <5%) are activated robustly during the task to elicit an immediate early gene (IEG), such as Fos, response and participate in such an ensemble [7]. These immediate early genes have been previously explored to be a proxy of synergistic glutamate and dopamine activity [6]. The majority of surrounding neurons are less activated and not directly involved in the specific task or behavior. Studies using fMRI do not measure the specific response from only the highly active neurons, but more likely reflect the activity of smooth muscle, epithelial cells, glia, and the less activated neurons. This is important because neuronal ensembles serve as the key mediators of highly specific learned

Abbreviations: fMRI, functional magnetic resonance imaging; FM-PAT, functional molecular photoacoustic tomography; IEG, immediate early gene; β-gal, beta-galactosidase; mPFC, medial prefrontal cortex; PTSD, post-traumatic stress disorder; dACC, dorsal anterior cingulate cortex; vmPFC, ventromedial prefrontal cortex; PL, prelimbic cortex; IL, infralimbic cortex; PA, photoacoustic; DMSO, dimethyl sulfoxide; PBS, phosphate-buffered saline; PFA, paraformaldehyde; TBS, tris-buffered saline; ANOVA, analysis of variance.

* Correspondence to: 3119 Integrative Bioscience Center (IBio), 6135 Woodward Ave, Detroit, MI 48202, USA.
E-mail address: sperrine@med.wayne.edu (S.A. Perrine).

https://doi.org/10.1016/j.pacs.2023.100551
Received 13 September 2022; Received in revised form 19 May 2023; Accepted 26 August 2023
Available online 27 August 2023

behaviors, including fear learning and discrimination [8–11], reward-based learning and food-seeking behavior [7, 12–15], and various drug and alcohol addiction-related models [6, 12, 13, 16–22].

Using optical excitation and acoustic detection, our functional molecular photoacoustic tomography (FM-PAT) system allows for direct imaging of neuronal ensembles with a large field-of-view (probe area 1.3 cm transversely by 2.2 cm depth) and high spatial resolution (axial and lateral resolutions of 250 μm and 480 μm, respectively) [23]. In a previous study using an *ex vivo* preparation of the brain of the Fos-LacZ transgenic rat, we showed that the application of X-gal, an exogenous prochromogenic molecule that when cleaved by beta-galactosidase (β-gal) that is co-expressed with Fos uniquely in the Fos-LacZ transgenic rat, produces a robust and selective FM-PAT signal [24]. This signal was present in cortical neurons highly activated by cocaine administration or a shock-tone paired stimulus compared to behaviorally naive control conditions. This demonstrated successful and direct detection of Fos-expressing neuronal ensembles *ex vivo* [24]. While the FM-PAT signal represented an average of the ensemble response in a given brain region, rather than allowing visualization of individual neurons, the FM-PAT signal resulted only from the highly active neurons and not from a more general neural response, as is measured using fMRI. Thus, FM-PAT is similar to optical imaging techniques that can measure direct molecular neuronal responses, typically through calcium imaging [25]. The current experiments expand this novel application further by demonstrating its abilities *in vivo* and paired with behavioral testing, thereby allowing us to explore the neurobiological role of the medial prefrontal cortex (mPFC) in conditioned fear behavior.

Fear-related psychopathologies such as post-traumatic stress disorder (PTSD) and select anxiety disorders are often assessed using conditioned fear testing [26]. This is often observed through overgeneralization of fear and/or failure to extinguish fear normally. Although the amygdala is perceived as central to fear learning, various studies have shown that other brain regions play key roles in the phases of fear learning, including acquisition, expression (memory recall), extinction, and extinction-retention (extinction recall) [27–31]. For example, increased neural activity in the dorsal anterior cingulate cortex (dACC) decreases extinction learning and exacerbates fear expression [30, 32–35]. The ventromedial prefrontal cortex (vmPFC) has dual effects, including increased neural activity when individuals expressed increased fear extinction recall and decreased fear expression [30, 31, 33–37]. In the rodent, the prelimbic cortex (PL) functions similarly to the dACC in humans and the infralimbic cortex (IL) functions similarly to the vmPFC [35]. The role of Fos-expressing ensembles has previously been investigated in conditioned fear behaviors, showing robust differences in neuronal activation in various brain regions including the mPFC after fear conditioning compared to control animals not undergoing fear learning [27,28,38]. Using FM-PAT *ex-vivo*, we have previously detected neuronal ensembles in the mPFC and its subregions that are activated upon a shock-tone pairing model akin to fear conditioning [24,39]. However, there are limited methods to study neuronal ensembles *in vivo* [3,4,40]. For this reason, we employed an established rat model of fear conditioning paired with the novel application of photoacoustic (PA) imaging *in vivo* to identify and quantify neuronal ensembles. This research aims to refine the role of neuronal ensembles in the acquisition of conditioned fear using FM-PAT in Fos-LacZ transgenic rats undergoing behavioral testing to detect and quantify neuronal ensembles in the mPFC and its subregions (PL and IL) *in vivo*.

In this study we hypothesized that during fear acquisition, unique neuronal ensembles would be activated in the mPFC and its subregions in comparison to behavioral and vehicle controls and these ensemble differences could be quantified using novel Fos-LacZ-enhanced PA imaging *in vivo*. We used a parallel group of rats analyzed through traditional *ex vivo* immunofluorescence techniques to spatially resolve and confirm the role of these activated mPFC neuronal ensembles. We compared the animals' behavioral responses in both groups to the degree of regional Fos ensemble activity to further validate FM-PAT and refine the roles of cortical subregions in learning behaviors.

2. Methods

2.1. Animals

We used 128 homozygous Fos-LacZ transgenic Wistar (Wistar-Tg (Fos-LacZ)1Ottc) rats of both sexes between eight to twelve weeks of age. These animals were originally developed by Dr. Tom Curran (currently at The Children's Mercy Hospital in Kansas City, Missouri). The rats were housed in a climate and humidity-controlled environment on a reversed light-dark cycle and bred in-house. Upon weaning, rats were separated by sex and pair-housed at Wayne State University's Division of Laboratory Animal Research (AAALAC-accredited) facilities. Eighty rats were used for *in vivo* FM-PAT in an experimental fear-conditioned group that received X-gal (n = 22, 12 females, 10 males), a non-shocked sham conditioned control group that received X-gal (n = 22, 13 females, 9 males), a behaviorally naive group that received X-gal (n = 19, 11 females, 8 males), and fear-conditioned vehicle control group (n = 17, 9 females, 8 males). Forty-eight rats were used for immunofluorescence microscopy in fear-conditioned (n = 16, 8 females, 8 males), non-shocked sham conditioned (n = 16, 8 females, 8 males), and behaviorally naïve (n = 16, 7 females, 9 males) groups. Handling and behavioral procedures were performed during the dark (active) phase of the rats' light cycle under dim red room light and fear conditioning chamber red light. All animals were allowed access to food and water *ad libitum* outside of time spent within the fear conditioning chambers or under anesthesia. All experiments were conducted in a climate and humidity-controlled behavioral-testing suite. All animals were handled and weighed for two days before experimentation. These procedures were approved by the Institutional Animal Care and Use Committee of Wayne State University in accordance with the *Guide for the Care and Use of Laboratory Animals* [41].

2.2. Experimental design

Fig. 1 illustrates the experimental timeline, the overall study design, and specific methods for the FM-PAT groups (I) and the immunofluorescence microscopy groups (II). As an overview, for both groups, rats were subjected to a standard fear conditioning paradigm or control conditions. For FM-PAT, rats were given an intrathecal injection of X-gal following fear conditioning, allowed 24 h for X-gal product to form in Fos-LacZ-expressing cells, and then prepared for FM-PAT by performing a partial craniotomy. Measurement of Fos neuronal ensembles in the mPFC was then conducted using FM-PAT *in vivo*. For immunofluorescent microscopy, rats were euthanized by transcardial perfusion following behavioral testing. Detailed methods of these procedures and statistical analyses are described next.

2.3. Fear conditioning or control conditions

Rats underwent acquisition of conditioned fear learning using a repeated sequence of tone and shock pairings similar to our previous publications [24,42] or control conditions. Fear conditioning chambers (25.5 ×30×29 cm, Med Associates Inc., St. Albans, Vermont, USA) consisted of modular aluminum sidewall panels, black and white striped front and back walls, an electrifiable grid floor, and the chambers were enclosed in sound-attenuating cubicles. Each chamber was illuminated by a red incandescent house light, had the chamber fan turned on, and was scented with 1% acetic acid in water. Female and male rats were tested at separate times and fear conditioning chambers were thoroughly cleaned with 70% ethanol in water between every testing session. One day before fear conditioning or non-shocked sham conditioning, animals were habituated for 10 min in the conditioning chambers. Behaviorally naive controls were only handled and weighed on this day. On test day, rats were placed into the chambers and after a

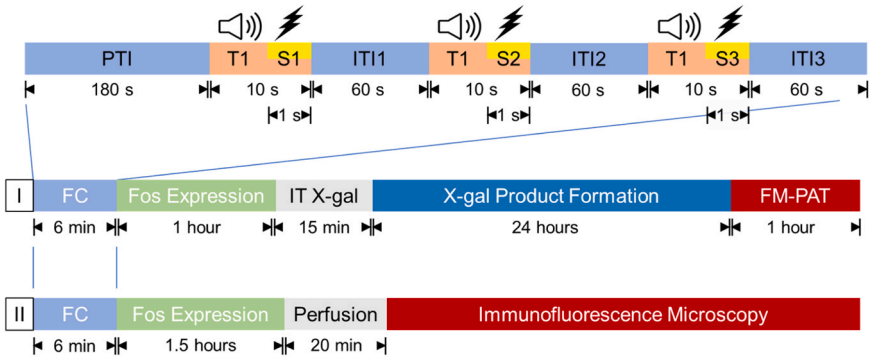

Fig. 1. Overall experimental timeline for *in vivo* FM-PAT (I) and *ex vivo* immunofluorescence microscopy (II) PTI: pretrial interval. The timeline for Fear conditioning (FC) is given detailing the three shock-tone pairings. T#: tone number, S#: shock number, ITI#: intertrial interval number, IT: Intrathecal.

180-second pre-trial period, they were exposed to three 10-second tones (2 kHz, 70 dB), with each tone co-terminating with a 1-second duration shock of 1.0 mA. The shock was omitted for non-shocked sham conditioned controls. Behaviorally naive controls were left undisturbed in their home cage on this day. Shock-tone pairings were separated by a 60-second intertrial interval (ITI), and the session ended 60-seconds after the last tone presentation. Videos of animal behavior were digitally recorded and thresholded inactivity state (*i.e.*, behavioral data) was measured using the Noldus EthoVision XT Behavior Recognition system (Leesburg, VA, USA) on the habituation and fear conditioning days. Data were acquired using Ethovision's "Activity" setting and averaged over 5 samples with an inactive threshold of 0.1%. The data from the entire habituation period, the entire pretrial interval, and the last 30 s of every ITI were used for the quantification of fear-related behavior. The last 30 s of the ITI was used as it provided sufficient separation from the animals' reactive movements to the delivery of the shock and a more specific freezing response as a measure of fear-like behavior.

2.4. Intrathecal injection and partial craniotomy for FM-PAT

We used the intrathecal route of administration to maximize brain levels of X-gal as it bypasses the blood-brain barrier. This procedure was adapted from previous publications [43–45]. We chose to inject rats 60 min following the end of fear conditioning or non-shocked sham conditioning, with behaviorally naive animals taken straight from home cages, because we experimentally determined that an additional 30 min was necessary for the intrathecally injected X-gal to reach the brain (data not shown). This allowed for the measurement of peak Fos expression at 90 min following experimental conditions [5,46]. Animals were anesthetized with isoflurane (4% induction and 1–2% maintenance in oxygen). The lumbar region of the rat was shaved. An area encompassing L3-L6 was sterilized with three rounds of alternating betadine and alcohol. The rat was secured in one hand by the pelvic girdle and a 25 Gauge x 2-cm needle attached to a 100 μL Hamilton syringe was inserted between the L5 and L6 vertebrae. While continuously securing the rat 0.2 mL/kg of X-gal dissolved in dimethyl sulfoxide (DMSO) or DMSO vehicle, which served as the fear-conditioned vehicle control group, was injected into the intrathecal space. Sudden and often repetitive movement of the tail and/or a sudden change in respiration were considered as indications of a successful injection [45]. It was critical that the rat was only lightly anesthetized to consistently observe these reactions to provide a successful injection of X-gal or vehicle control. The syringe was gently removed following the administration of X-gal or vehicle control over 30-seconds, and the injection site was then cleaned using sterile 70% alcohol prep pads. The rats were monitored post-injection for any adverse effects. Occasionally animals experienced short-term paralysis of hind limbs that resolved within minutes post-injection. Once any temporary paralysis subsided, animals were returned to their home cages to allow for X-gal conversion in Fos-LacZ expressing cells. In cases of continued paralysis, the animal was monitored for an extended period of 6 h.

Twenty-four hours following intrathecal injection of X-gal or vehicle control, the rats were anesthetized with isoflurane (4% induction, 2% maintenance in oxygen), and the skin covering their skull was shaved. Each rat was secured using a stereotaxic frame (American Standard Instruments, Warren, Michigan, USA) with anesthesia attachment. Once secured to the frame, the anterior scalp was removed using blunt surgical scissors. The skull was revealed, and connective tissue was removed using a sterile cotton swab (Q-tip). Sterile saline and gauze were used to clean the skull surface and surrounding tissue. To perform the craniotomy, a Foredom K.1070 High-Speed Rotary Micromotor Kit (Blackstone Industries LLC, Bethel, CT, USA) was used to cut a 5 mm diameter hole centered over the mPFC (+ 3.0 mm AP, midline, relative to bregma, Fig. 2A-B). The detached skull piece was then gently removed using blunt forceps to expose the underlying dura. The exposed dura was cleaned using sterile saline and gauze and any bleeding was cleaned before proceeding to PA imaging.

2.5. FM-PAT

The PA imaging system used for FM-PAT consists of three major components: (1) A 128-element 18.5 MHz linear array ultrasound transducer (L22–14v, Vermon Inc., Tours, France) to detect PA signal, (2) a 10 Hz pulsed and tunable Nd:Yag laser, (Opotek Phocus HE MOBILE, OPOTEK, LLC, USA) coupled with a custom made bifurcated fiber optic cable from Fiberoptics Technology Inc. (Pomfret, CT, USA) to generate and deliver the optical energy at a maximum of 20 J/cm^2, and (3) a high-frequency ultrasound research platform (Vantage 128, Verasonics Inc., Kirkland, WA, USA) for data acquisition, image reconstruction, and post-processing [47,48]. Detailed technological parameters of the PA system components have been described previously in [24]. For efficient acoustic coupling, ultrasound gel was applied to the clean dural surface of the rat brain and the ultrasound transducer active sensing area [49]. The ultrasound transducer was fitted with custom 3-D printed fiber optic bundle holders and attached to the stereotaxic frame. The ultrasound transducer was centered over the craniotomy (+3.0 AP, 0, +5.0 DV) using ultrasound anatomical markings to confirm the positioning of the probe. Once the probe was in place, the brain of each anesthetized animal was rapidly scanned using our PA setup (Fig. 2C-D). A 2-D PA image slice in the coronal plane of the mPFC was acquired at the wavelengths of 690, 725, 750, 800, and 912 nm. 40 image frames were recorded at each wavelength with an accompanying ultrasound image (*i.e.*, 200 PA images and 1 ultrasound image in total per rat). Data acquisition and processing were performed using a customized MATLAB script for L22–14v transducer array. The energy at the output of the optical parametric oscillator (OPO) was monitored and recorded through the internal energy monitor during the scan. Anesthetized animals were immediately euthanized following the completion of the

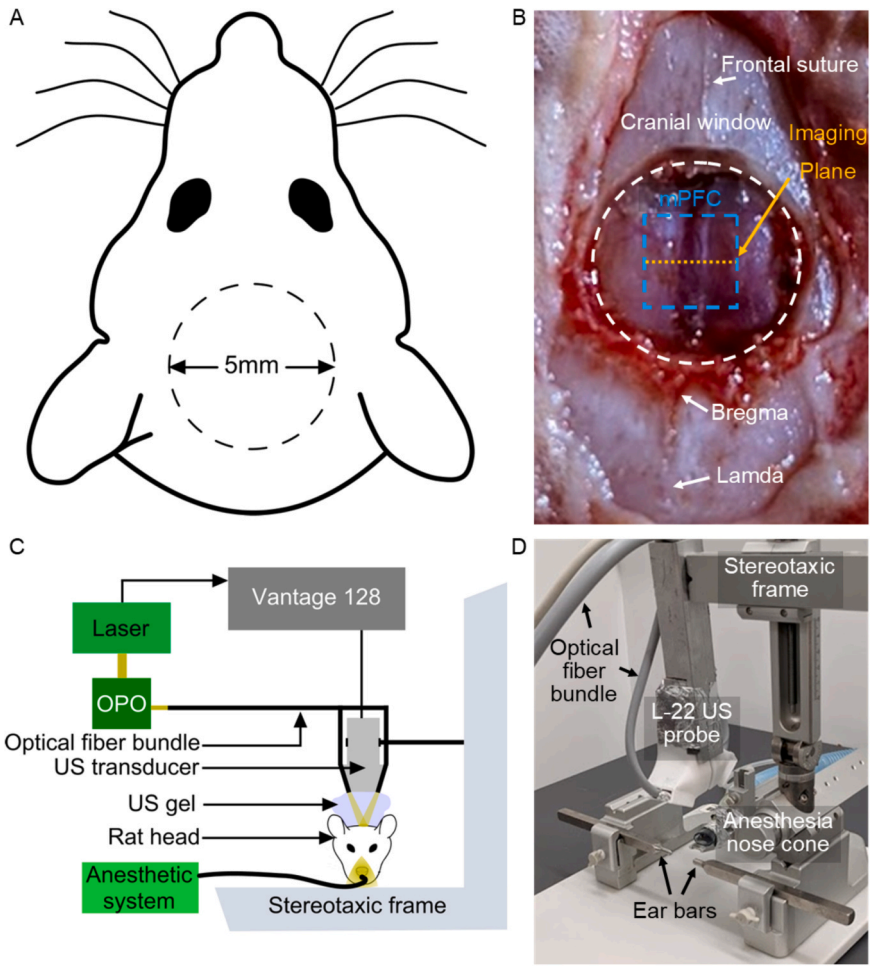

Fig. 2. A: Schematic of the cranial window showing approximate position on rat head. B: Picture of 5 mm craniotomy over the medial prefrontal cortex (mPFC). C: Diagram of photoacoustic imaging setup. D: Picture of FM-PAT setup with imaging probe and anesthesia in place. OPO: optical parametric oscillator, DAQ: data acquisition, L-22 US probe: L22–14v ultrasound transducer.

imaging session.

To compensate for pulse-pulse and wavelength-based optical energy fluctuation, all collected PA images were linearly corrected by the laser energy recorded at the time of imaging specific to the wavelength used. Images with motion artifacts were identified by an experimenter blind to the groups and subsequently replaced using averaged images of the remaining motion-free images of the corresponding wavelength for the respective rat. A custom MATLAB script was used to recreate X-gal product signal images using multispectral optical tomography (MSOT) processing [50] on five averaged images produced from 40 images collected at each respective wavelength. Brain regions of interest were then automatically quantified based on the averaged and normalized pixel intensity of the MSOT-derived X-gal product map within the measured areas and size-adjusted by sex given that males are overall larger, both in terms of body and brain, than females despite their similar ages at the time of the experiment [51]. The PL and IL subregions were differentiated by using their known anatomical positions guided by landmarks such as the surface of the skull and landmarks visible *via* ultrasound (*i.e.*, the brain's white matter tracks) [52].

2.6. Perfusion and ex vivo tissue preparation

Each rat within the immunofluorescence microscopy groups underwent transcardial perfusion followed by brain extraction and post-fixation 90 min after the conclusion of behavioral testing. Isoflurane anesthetized rats were perfused through the left ventricle with phosphate-buffered saline (PBS) at a flow rate of 30 mL/min for 5 min and then with 4% paraformaldehyde (PFA) in PBS for 15 min. Brains were removed, post-fixed in 4% PFA for 24 h, cryoprotected with 30% sucrose in PBS, and then frozen by submersion in chilled isopentane. Isopentane was maintained at − 30 °C to − 40 °C *via* the direct addition of dry ice. Brains were then cut into 40-micron coronal sections, washed (3 ×10 min in tris-buffered saline (TBS)), incubated in a blocking buffer (TBS with 0.2% Triton X and 3% Normal Donkey Serum; Sigma-Aldrich, St. Louis, MO, USA), and then incubated with 1:100 phospho-c-Fos anti-rabbit (#5348; Cell Signaling, Danvers, MA, USA) and 1:1000 β-gal anti-mouse antibodies (sc-65670, Santa Cruz Biotechnology Inc, Santa Cruz, CA, USA) in blocking buffer while rocking at 4 °C for 48 h. Then the brain sections containing the mPFC were washed and incubated with 1:200 donkey anti-rabbit Alexa 488 (A21206, Invitrogen, Carlsbad, CA, USA) and 1:200 donkey anti-mouse Alexa 568 antibodies (A10037, Invitrogen, Carlsbad, CA, USA) in the blocking buffer for one hour. Next, the sections were washed and incubated with 1:200 RBFOX3/NeuN antibody [Alexa Fluor® 405] (1B7, Novus Biologicals, Littleton, CO, USA) in the blocking buffer for 24 h. Sections were then washed and mounted onto Fisherbrand Superfrost Plus Microscope Slides (12–550–15, Fisher Scientific, Waltham, MA, USA), coverslipped using Vectashield HardSet Antifade Mounting Media (H-1400, Vector Laboratories, Burlingame, CA, USA), and protected from light at 4 °C until slices were imaged using the THUNDER Imager 3D Live Cell & 3D Cell Culture & 3D Assay (Leica Microsystems, Buffalo Grove, IL, United States). Representative microscopy images shown in Fig. 5 were

enhanced for easy reader visualization using the internal software of the THUNDER Imager 3D Live Cell & 3D Cell Culture & 3D Assay (Leica Microsystems, Buffalo Grove, IL, United States). Raw microscopy images were quantified for positive cell count using the FIJI distribution of ImageJ software [53]. Cells were identified using a set percentage threshold at every channel. Fos was set at a 5% threshold and β-gal was set at a 10% threshold. The range for cell size was 30–1000 μm and the range for circularity was 0.25–1.00. The preceding parameters were selected to minimize the effect of artifacts and maximize accuracy compared to a manual count. NeuN was used as a neuronal marker to confirm the presence and specificity of Fos and β-gal to neurons (data not shown). Regions of interest were applied in accordance with "The Rat Brain In Stereotaxic Coordinates" by Paxinos and Watson [52]. These were then saved so that identical regions of interest could be applied to each channel for replication. Raw data were collected for neuronal cell count, average cell size, and the total and percentage area of the region covered by cells. The area of the region used to calculate cell count/mm^2 was derived using the total and percentage area of the region covered by cells.

2.7. Statistical Analysis

Prior to analysis, the data were reviewed for outliers and quality problems. One statistical outlier was excluded from the immunofluorescence groups because of experimental concerns regarding an accidental potentially Fos-provoking disturbance by laboratory personnel (behaviorally naive animal, male, >2.5 SD from the mean). Automatic scanning focusing errors, imaging artifacts, and staining inconsistencies led to the exclusion of five animals from the immunofluorescence groups (two behaviorally naive, two non-shocked sham conditioned, and one fear conditioned animal). Five animals were excluded from the FM-PAT groups: one animal was euthanized due to continued paralysis after intrathecal injection (female fear conditioned animal), one rat was found dead on the craniotomy day (male non-shocked sham conditioned animal), two animals died during the craniotomy procedure (one male non-shocked sham conditioned and one male behaviorally naive animal), and one rat was excluded due to illumination abnormalities, where the raw photoacoustic images had a higher-than-expected signal both in the ROI and the background, observed after review of the PA images (male behaviorally naive animal).

After verification of the quality of the data, all analyses were initially assessed with a multi-way ANOVA including sex as a predictor variable. However, no significant interaction with sex was observed in any analysis, therefore, we simplified our overall analysis and presentation of the results by collapsing data to omit sex as a variable. A repeated-measures ANOVA was used to analyze the experimental group's freezing conditioned fear behavior within the session. A group-wise univariate Welch's ANOVA was used to interpret *post hoc* differences of the normalized MSOT-derived X-gal product pixel intensity (FM-PAT derived X-gal Product signal) contained within the mPFC across the experimental group. The number of Fos or β-gal positive stained cells/mm^2 contained within the mPFC, and X-gal product and immunofluorescence in fear conditioned and non-shocked sham conditioned groups were transformed into a percent change from their respective behaviorally naive groups. These percentage changes across imaging modalities were then tested using univariate ANOVA. A 2-way ANOVA using group and subregion as factors was used to test the X-gal product within the PL and IL mPFC subregions. These statistical analyses were repeated to test the number of Fos or β-gal positive stained cells/mm^2 contained within the PL and IL mPFC subregions. Correlations were used to test the Fos expression compared to the β-gal expression for mPFC and its subregions. In all cases, significance was set at $p < 0.05$. The familywise error rate was controlled in *a priori* and *post hoc* hypothesis testing using the Benjamini–Hochberg method with a false discovery rate of 0.05 [54]. The Benjamini–Hochberg method was chosen to limit the false discovery rate without a dramatic expansion in the type II error rate given the exploratory and inherent repetition of the study measures. Specific comparisons are detailed in the Results (Section 3).

3. Results

3.1. Fear Acquisition

The repeated-measures ANOVA of the fear-conditioned and non-shocked sham conditioned groups revealed an overall significant time and group interaction in the freezing response ($F(3, 273) = 14.81$, $p < 0.0001$). The effect of time ($F(3, 273) = 62.60$, $p < 0.0001$) and group ($F(1, 91) = 9.34$, $p < 0.001$) was significant. *Post hoc* analysis revealed significance remained after Benjamini–Hochberg correction in the difference of percent time spent freezing between the fear-conditioned and non-shocked sham conditioned groups at the 2nd ($p = 0.0034$) and 3rd ITIs ($p < 0.0001$) (Fig. 3).

3.2. FM-PAT

Images of the mPFC and its IL and PL subregions were generated for quantification with averaged representative images provided for each group (Fig. 4A-D). Normalized X-gal product intensity (arbitrary units) was analyzed using a univariate Welch's ANOVA with *post hoc* unpaired t-tests with Welch's correction were used to determine differences between the vehicle control, behaviorally naive, non-shocked sham conditioned, and fear-conditioned groups. The ANOVA resulted in an overall significant group effect in the whole mPFC ($F(3, 38.94) = 4.510$, $p = 0.008$). *Post hoc* comparisons revealed significant differences remained after Benjamini–Hochberg correction in normalized X-gal product intensity (arbitrary units) between the vehicle control and non-shocked sham conditioned groups (uncorrected $p = 0.019$), the vehicle control and fear-conditioned groups (uncorrected $p = 0.027$), the behaviorally naive and non-shocked sham conditioned groups (uncorrected $p = 0.008$), and the behaviorally naive and fear-conditioned groups (uncorrected $p = 0.011$). As expected, no significant difference was observed between the vehicle control and behaviorally naive group in X-gal product intensity in the mPFC (uncorrected $p = 0.818$). Surprisingly, no differences were observed between non-shocked sham conditioning and fear conditioning groups (uncorrected $p = 0.880$ (Fig. 4E).

The PL and IL were analyzed using 2-way ANOVA with the experimental group and mPFC subregion as the factors. Both experiment group and subregion were significant overall as independent factors ($F(3, 142) = 5.55$, $p = 0.0012$), $F(1, 142) = 13.76$, $p = 0.0003$, respectively). There was no significant interaction between the group and subregion (F

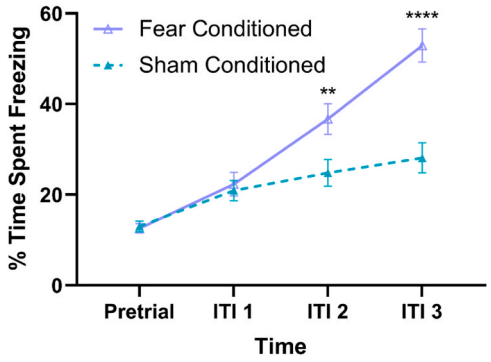

Fig. 3. Fear acquisition data displaying freezing behavior changes measured through the percentage of time spent freezing during the pretrial period and the second half of each intertrial interval (ITI). Repeated-measures ANOVA of the fear response in FC animals demonstrated a significantly higher percentage of time freezing after the second and third shock-tone pairings. * : Significant after Benjamini–Hochberg with uncorrected p values * *$p < 0.01$, * ** *$p < 0.0001$.

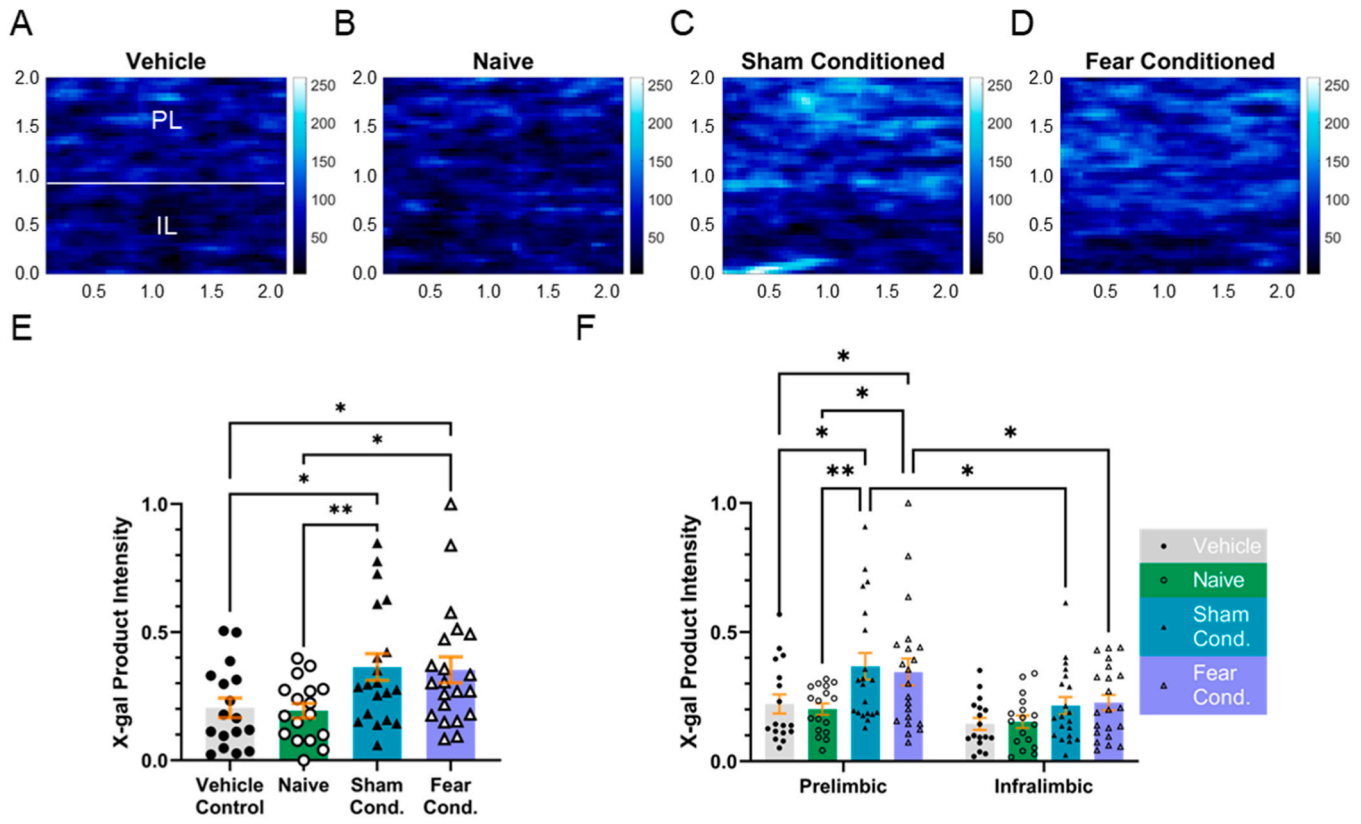

Fig. 4. A: Representative averaged MSOT-derived X-gal product image of a vehicle control animal. Prelimbic (PL) and infralimbic (IL) cortex subregions are labeled. Image scale given in mm. Color-bar scale: 0–255 intensity units. B: Representative averaged X-gal product image of a behaviorally naive animal. C: Representative averaged X-gal product image of a non-shocked sham conditioned animal. D: Representative averaged X-gal product image of a fear conditioned animal. E: Comparison of each FM-PAT group's mPFC X-gal product intensity (normalized arbitrary units) analyzed with univariate Welch's ANOVA. F: Comparison shown for PL and IL subregions of the mPFC analyzed using 2-way ANOVA with the experimental group and mPFC subregion as the factors. * : Significant after Benjamini–Hochberg with uncorrected p values *p < 0.05, * *p < 0.01.

(3142) = 0.7216, p = 0.5407). Planned comparisons, based on findings in the mPFC, revealed significant differences remained after Benjamini–Hochberg correction in x-gal product intensity (arbitrary units) within the PL between the vehicle control and non-shocked sham conditioned groups (uncorrected p = 0.0073), vehicle control, and fear-conditioned groups (uncorrected p = 0.0210), the behaviorally naive and non-shocked sham conditioned groups (uncorrected p = 0.0024), and the behaviorally naive and fear-conditioned groups (uncorrected p = 0.0076). The IL had no significant differences remained after Benjamini–Hochberg correction in X-gal product intensity (arbitrary units) between the vehicle control and non-shocked sham conditioned groups (uncorrected p = 0.1866), the vehicle control and fear-conditioned groups (uncorrected p = 0.1218), the behaviorally naive and non-shocked sham conditioned groups (uncorrected p = 0.2447), or the behaviorally naive and fear-conditioned groups (uncorrected p = 0.1649). Significant inter-subregional differences remained after Benjamini–Hochberg correction in X-gal product intensity (arbitrary units) were observed between the PL and IL in the sham conditioned (uncorrected p = 0.0037) and the fear-conditioned (uncorrected p = 0.0198) groups. However, no significant differences remained between the PL and IL in the vehicle control (uncorrected p = 0.3850) or behavioral naive (uncorrected p = 0.1694) groups (Fig. 4F).

3.3. Immunofluorescence microscopy

NeuN, Fos, and β-gal triple labeled immunofluorescence images of the mPFC and IL and PL subregions were analyzed for neuronal cell count quantification (Fig. 5A-B). The univariate ANOVA of the Fos^+ cell count per mm^2 for the behaviorally naive, non-shocked sham conditioned, and fear-conditioned groups resulted in an overall significant group effect in the whole mPFC (F(2, 38) = 9.321, P = 0.0005). *Post hoc* comparisons of the mPFC revealed a significant difference remained after Benjamini–Hochberg correction in Fos^+ cell count per mm^2 between the behaviorally naive and non-shocked sham conditioned groups (uncorrected p = 0.0005) and between the behaviorally naive and fear-conditioned groups (uncorrected p = 0.0007). Confirming what was observed with FM-PAT, no differences were observed between non-shocked sham conditioning and fear conditioning groups (uncorrected p = 0.7713) (Fig. 5C). The univariate ANOVA of the $\beta\text{-gal}^+$ cell count per mm^2 for the behaviorally naive, non-shocked sham conditioned, and fear-conditioned groups resulted in an overall significant group effect in the whole mPFC (F(2, 38) = 4.567, P = 0.0167). *Post hoc* comparisons of the mPFC revealed a significant difference remained after Benjamini–Hochberg correction in $\beta\text{-gal}^+$ cell count per mm^2 between the behaviorally naive and non-shocked sham conditioned groups (uncorrected p = 0.0226) and between the behaviorally naive and fear-conditioned groups (uncorrected p = 0.0075). Confirming what was observed with FM-PAT and Fos^+ neuron count, no differences were observed between non-shocked sham conditioning and fear conditioning groups (uncorrected p = 0.7161) (Fig. 5E).

The Fos^+ cell count per mm^2 in the PL and IL were analyzed using 2-way ANOVA with the experimental group and mPFC subregion as the factors. Both experiment group and subregion were significant overall as independent factors (F(2, 76) = 16.60, p < 0.0001), F(1, 76) = 7.471, p = 0.0078, respectively). There was no significant interaction between the group and subregion (F(2, 76) = 0.3489, p = 0.7066). Planned comparisons revealed significant differences remained after Benjamini–Hochberg correction in Fos^+ cell count per mm^2 within the PL

between naive control and non-shocked sham conditioned groups (uncorrected $p < 0.0001$) and between naive control and fear-conditioned groups (uncorrected $p = 0.0002$). The IL had significant differences remained after Benjamini–Hochberg correction in Fos^+ cell count per mm^2 between the naive control and non-shocked sham conditioned groups (uncorrected $p = 0.0027$) and between the naive control and fear-conditioned groups (uncorrected $p = 0.0041$). Despite an overall significant F test, no significant interregional differences remained after Benjamini–Hochberg correction in Fos^+ cell count per mm^2 between the PL and IL in the naive control (uncorrected $p = 0.3878$), sham conditioned (uncorrected $p = 0.0582$) or the fear-conditioned (uncorrected $p = 0.0522$) groups (Fig. 5D).

The β-gal $^+$ cell count per mm^2 in the PL and IL subregions were analyzed using 2-way ANOVA with the experimental group and mPFC subregion as the factors. Both experiment group and subregion were significant overall as independent factors ($F(2, 76) = 7.939$, $p = 0.0007$), $F(1, 76) = 5.003$, $p = 0.0282$, respectively). There was no significant interaction between the group and subregion ($F(2, 76) = 0.3141$, $p = 0.7314$). Planned comparisons revealed significant differences remained after Benjamini–Hochberg correction in β-gal $^+$ cell count per mm^2 between the naive control and non-shocked sham conditioned groups (uncorrected $p = 0.0088$) and between naive control and fear-conditioned groups (uncorrected $p = 0.0025$) in the PL. The IL had no significant differences remained after Benjamini–Hochberg correction in β-gal $^+$ cell count per mm^2 between the naive control and non-shocked sham conditioned groups (uncorrected $p = 0.0938$) or between the naive control and fear-conditioned groups (uncorrected $p = 0.0332$). Despite an overall significant F test, no significant intersubregional differences remained after Benjamini–Hochberg correction in β-gal $^+$ cell count per mm^2 between the PL and IL in the naive control (uncorrected $p = 0.5354$), sham conditioned (uncorrected $p = 0.1105$), or the fear-conditioned (uncorrected $p = 0.1001$) groups (Fig. 5F).

As anticipated, correlation analysis of the Fos^+ cell count per mm^2 *vs* the $β\text{-gal}^+$ cell count per mm^2 regardless of group resulted in a significant correlation in the mPFC ($F(1,39) = 111.6$, $R = 0.8608$, $p < 0.001$), the PL ($F(1,39) = 122.8$, $R = 0.8712$, $p < 0.001$), and the IL ($F(1,39) = 70.73$, $R = 0.8029$, $p < 0.001$) (Fig. 5G).

3.4. FM-PAT and Immunofluorescence Comparison

The percent difference of FM-PAT-derived normalized X-gal product intensity in the non-shocked sham conditioned (Fig. 6A) and fear-conditioned (Fig. 6B) animals from the behaviorally naive group means was compared to the percent difference of Fos^+ or $β\text{-gal}^+$ cell count per mm^2 from their respective behaviorally naive group means. This created a cross-platform analysis where we could directly compare FM-PAT and immunofluorescence quantifiable outcomes.

The univariate ANOVA of the non-shocked sham conditioned normalized X-gal product intensity (outcome of FM-PAT), Fos^+ cell count per mm^2, and $β\text{-gal}^+$ cell count per mm^2 as a percentage difference from their respective behaviorally naive group means, resulted in an overall significant group effect in the IL ($F(2, 43) = 4.251$, $p = 0.021$), but no significant group effects were observed in the whole mPFC ($F(2, 43) = 1.571$, $p = 0.08411$) or the PL ($F(2,43) = 1.988$, $p = 0.149$). *Post hoc* analysis of the IL revealed that Fos^+ cell count per mm^2 diverged from both X-gal product intensity and $β\text{-gal}^+$ cell count per mm^2 by means of significant differences that remained after Benjamini–Hochberg correction in percentage difference from the behaviorally naive group between the X-gal product intensity and Fos^+ cell count per mm^2 (uncorrected $p = 0.009$) and between the Fos^+ cell count per mm^2 and the $β\text{-gal}^+$ cell count per mm^2 (uncorrected $p = 0.024$). No significant difference was observed between normalized X-gal product Intensity and $β\text{-gal}^+$ cell count per mm^2 (uncorrected $p = 0.863$) (Fig. 6A) demonstrating stronger agreement between X-gal product intensity and $β\text{-gal}^+$ cell count per mm^2.

The univariate ANOVA of the fear-conditioned normalized X-gal product intensity (FM-PAT's outcome), Fos^+ cell count per mm^2, and $β\text{-gal}^+$ cell count per mm^2 as a percentage difference from their respective behaviorally naive group means resulted in an overall significant group effect in the IL ($F(2, 48) = 3.277$, $p = 0.046$), but no significant group effects were observed in the whole mPFC ($F(2, 48) = 1.102$, $p = 0.341$) or the PL ($F(2,48) = 1.270$, $p = 0.290$). Despite a significant F-test, *post hoc* analysis of the IL revealed no significant differences remained after Benjamini–Hochberg correction in percentage difference from behaviorally naive group between the normalized X-gal product intensity and Fos^+ cell count per mm^2 (uncorrected $p = 0.019$), between the Fos^+ cell count per mm^2 and the $β\text{-gal}^+$ cell count per mm^2 (uncorrected $p = 0.054$) or between normalized X-gal product intensity and $β\text{-gal}^+$ cell count per mm^2 (uncorrected $p = 0.765$) (Fig. 6B).

4. Discussion

This study utilized two parallel cohorts of animals to establish FM-PAT as a technique for imaging Fos-expressing ensembles *in vivo*. The first cohort tested the capability of FM-PAT to image ensembles *in vivo*, and the second cohort validated the Fos-based measurements using immunofluorescence. We observed similar patterns of group differences between experimental cohorts. When analyzed as a percent difference from their respective naive control groups, our data show that FM-PAT accurately tracked the amount of β-gal present from the transgenic rats and β-gal expression was found to be highly correlated to Fos expression. These findings suggest that FM-PAT can provide an accurate measurement of Fos expression using the Fos-LacZ transgenic rat model.

Fear conditioning in rodents induces Fos expression in the mPFC [9,27,28,38] and therefore, we used it as an ideal paradigm to test FM-PAT's utility to detect neuronal activation. Animals across all shocked groups demonstrated progressive acquisition of conditioned fear after three shock-tone pairings in a controlled context (see Fig. 3). Both FM-PAT and immunofluorescence results support that the Fos signal is increased in the mPFC in both the sham- and fear-conditioned animals when compared to the behaviorally naive or the vehicle control groups. We hypothesize that both the sham and fear conditioning paradigms exposed animals to the novelty of the tones, and perhaps the context despite habituation, led to a high magnitude of Fos expression in both groups [55–57]. However, some subtle differences may exist in the expression patterns of the Fos-based neuronal ensembles (Fig. 4A-D) between the fear-conditioned and sham conditioned groups that will be discernable as this technology develops and matures. In fact, differential clustering of Fos-based neuronal activity is visually evident in the average PA-images presented in Fig. 4 with the fear-conditioned group having lateral clustered areas of high-intensity activity and sham-conditioned displaying a more medial, diffuse area of high-intensity within the mPFC.

To compare results across experiments, when X-gal product intensity and immunofluorescence cell counts were determined as a proportion of their respective naive control groups, we found limited evidence in the sham and fear-conditioned IL subregion that FM-PAT aligned closer with $β\text{-gal}^+$ cell count density results as compared to Fos (Fig. 6). This is not an unexpected outcome as the PA signal is directly dependent on the reporter gene system where transgene expression can vary slightly across brain regions [58] as we observed with a non-perfect correlation between Fos^+ and $β\text{-gal}^+$ cell count/mm^2 mainly in the IL (Fig. 5G).

In general, our results comparing the activity between the PL and IL contribute evidence that the activation in the PL was driving the mPFC response more than the IL in both sham and fear conditioning conditions. The 2-way ANOVA results indicated that the subregion was a significant factor in FM-PAT, Fos^+ cell count, and $β\text{-gal}^+$ cell count supporting a predominant role of the PL. However, *post hoc* analyses only revealed individual significant reductions in signal between the PL and the IL with the sham and fear-conditioned groups from the FM-PAT analysis (Fig. 4), and marginal effect ($p \approx 0.1$) for Fos^+ cell count and $β\text{-gal}^+$ cell count between PL and IL (Fig. 5). The main findings in all of

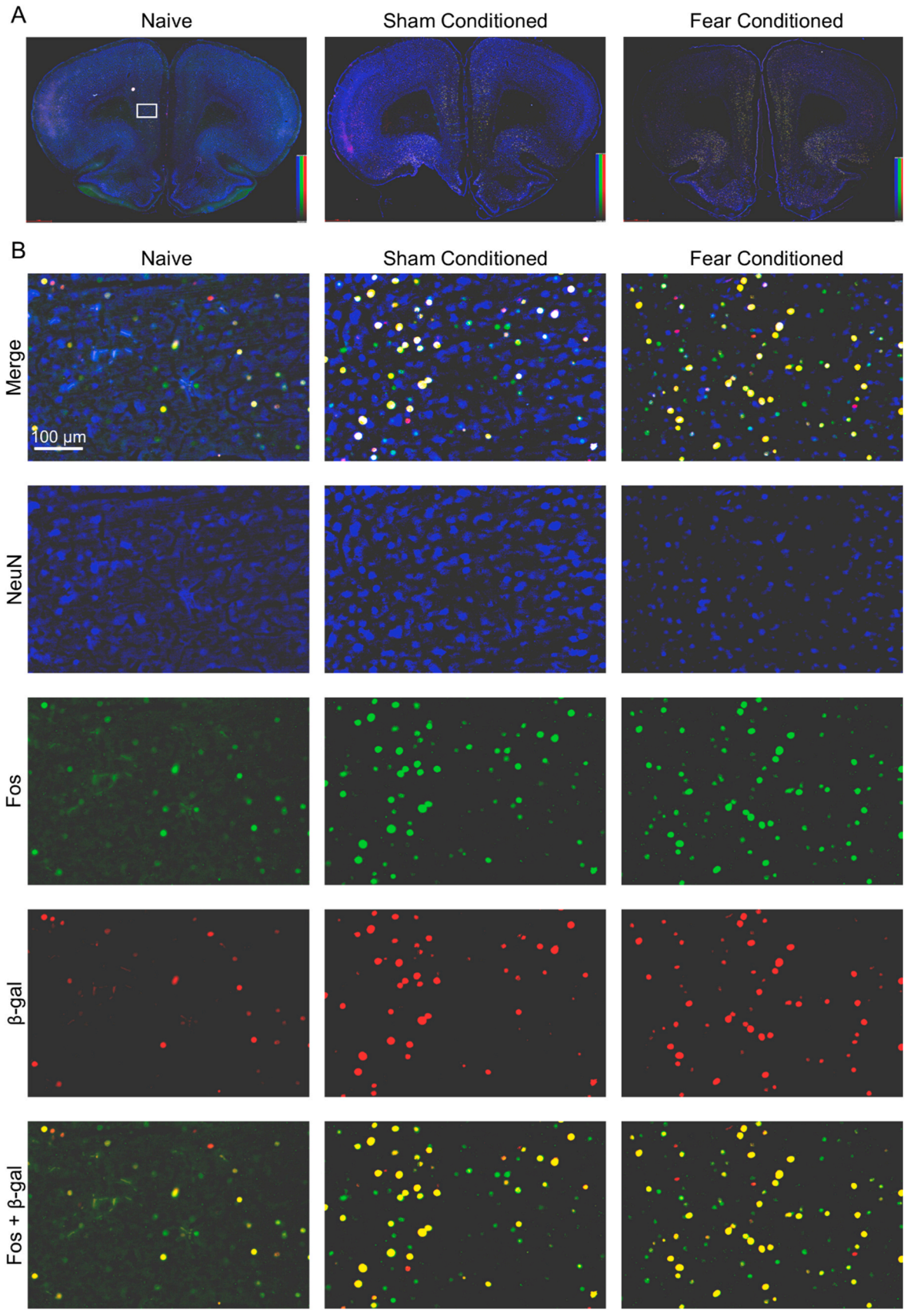

Fig. 5. A: Representative 200 x merged full-size Fos/β-gal/NeuN medial prefrontal cortex (mPFC) images across behaviorally naive, non-shocked sham conditioned, and fear-conditioned groups. The area shown in B is indicated by a white box. B: Representative 200 x Fos/β-gal /NeuN immunofluorescence microscopy images across behaviorally naive, non-shocked sham conditioned, and fear-conditioned groups C: Comparison of each group's Fos^+ cell count/mm^2 in the mPFC analyzed using univariate ANOVA. D: Comparison of each group's Fos^+ cell count/mm^2 in the subregions of the mPFC: the prelimbic and infralimbic cortices using 2-way

ANOVA with the experimental group and mPFC subregion as the factors. E: Comparison of each group's β-gal$^+$ cell count/mm^2 in the mPFC analyzed using univariate ANOVA. F: Comparison of each group's β-gal$^+$ cell count/mm^2 in the subregions of the mPFC: the prelimbic and infralimbic cortices using 2-way ANOVA with the experimental group and mPFC subregion as the factors. G: Linear regression of Fos$^+$ cell count/mm^2 *vs* β-gal$^+$ cell count/mm^2. Analyses are shown for the mPFC and its subregions: the prelimbic and infralimbic cortices. * : Significant after Benjamini–Hochberg with uncorrected p values *p < 0.05, * *p < 0.01, * **p < 0.001, * ** *p < 0.0001. All displayed correlations significant at the * **p < 0.001 level.

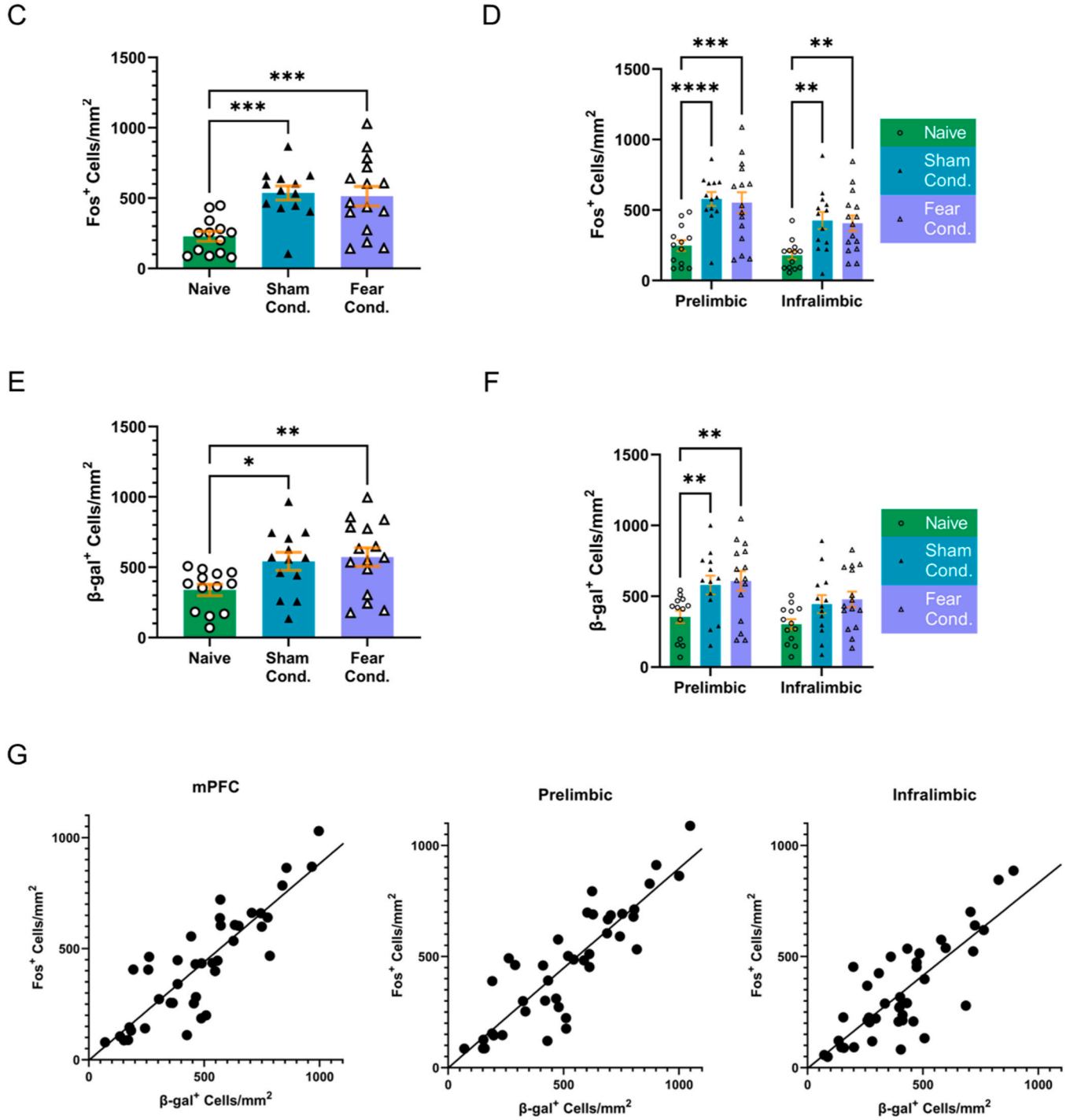

Fig. 5. (*continued*).

our experiments and the *post hoc* analysis of PA data support current literature that suggests neuronal activity in the PL regulates the acquisition of learned behaviors, particularly a conditioned fear response [30,37,59]. However, given our sham-conditioned groups also displayed a subregional-based difference, the role of fear learning remains to be clarified. The unique findings of FM-PAT demonstrating significant *post hoc* group differences may indicate that its measurement of intensity, which is related to total Fos-expression, may be more sensitive to subregional differences than changes in Fos/β-gal$^+$ cell count.

In this study, we expanded on our initial proof of principle study [24] by developing and demonstrating the capabilities of using FM-PAT in tandem with the Fos-LacZ transgenic rat model to quantify Fos-expressing neuronal ensemble activity after fear acquisition *in vivo*. Our previous work developed and tested this system and its ability to

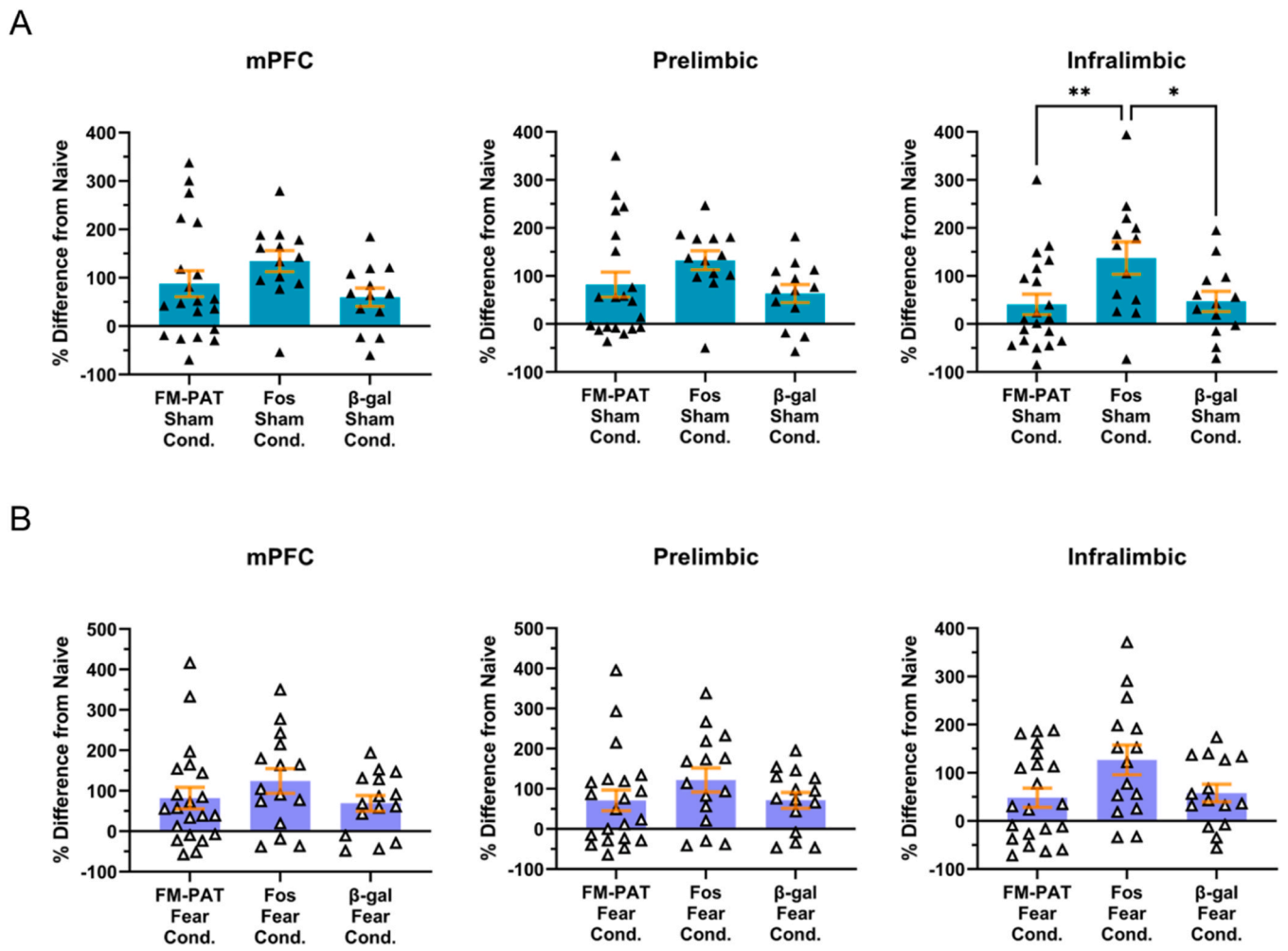

Fig. 6. Comparison across A: non-shocked sham conditioned and B: fear-conditioned FM-PAT and immunofluorescence results calculated as a percent difference from their respective behaviorally naive groups analyzed using univariate ANOVA. The comparison is shown for the mPFC and PL and IL subregions. * : Significant after Benjamini–Hochberg with uncorrected p values *$p < 0.05$, * *$p < 0.01$.

detect stimuli-driven Fos expression largely *ex vivo* or preliminarily *in vivo* [24,39]. This study expanded this work by bringing FM-PAT fully *in vivo* with a comprehensive study that integrated both behavioral and vehicle controls complete with comparisons to a parallel-designed immunofluorescent study *ex vivo* that is a current standard model for Fos detection. Prior approaches have conducted *in vivo* Fos visualization using invasive implanted fiber-optic cannula imaging [60] or low-resolution magnetic resonance contrast agents [61]. Researchers have also used calcium- or voltage-sensitive dye contrast agents in combination with PA imaging to track neural ensembles in an anesthetized mouse [3,4]. Our technique expands the utility of PA in ensemble identification further by selectively identifying Fos-expressing ensembles. Currently, the PA imaging technique used in this study represents an average of the Fos-expression across a brain region, but recent advances in photoacoustic microscopy may allow the expansion of the technique towards spatial resolutions capable of individual Fos-expressing cell imaging [62,63]. The advantage of imaging Fos-expressing neuronal ensembles over voltage- or calcium-based ensembles is that Fos-expressing ensembles provide a snapshot of the most persistently activated and highly involved neurons that are engaged in the behavior. In the future, both these exogenous chromophore techniques and endogenous chromophore techniques (*i.e.*, BOLD-response, lipid content, water content) could potentially be performed simultaneously using PA MSOT to differentiate the various chromophores involved. This type of multimodal neural and neuronal activity monitoring would provide a comprehensive model of neuroactivity behind a variety of behavioral and neuropsychological processes. In addition, FM-PAT is not necessarily a lethal imaging technique and may provide a future means for longitudinal imaging of Fos-expressing neuronal ensembles which would add considerable utility to neuronal ensemble research.

In summary, we demonstrated the ability of FM-PAT to accurately detect Fos-expressing ensembles within the mPFC and its subregions after fear conditioning. In combination with other existing and developing functional PA imaging techniques, FM-PAT may provide a broadly applicable way to monitor neuronal activity.

Funding

This work was supported by the National Institutes of Health [R01DA042057-Perrine, R01EB027769-Avanaki, R01EB028661-Avanaki, ZIADA000467-Hope, F30MH122093-Matchynski, R21DA052657-Perrine/Avanaki] and the U.S. Department of Veterans Affairs [I01RX002252-Perrine, I21RX002900-Conti].

CRediT authorship contribution statement

The authors confirm the following contributions to the paper: study conception and design: JIM, SK, CLA, BTH, KA, ACC, and SAP; data collection: JIM, TSC, NS, KMM, MW, ARW, and SK data analysis: JIM,

CLA, ACC, and SAP; interpretation of results: JIM, BTH, KA, ACC, and SAP; draft manuscript preparation: JIM, KA, ACC, and SAP. All authors reviewed the results, approved the final version of the manuscript, and agreed to be accountable for the research.

Declaration of Competing Interest

The authors declare that they have no known competing financial interests or personal relationships that could have appeared to influence the work reported in this paper.

Data Availability

Data will be made available on request.

Acknowledgment

We extend special thanks to Drs. Yan Yan and Mohammad Mehrmohammadi for their technological support during these experiments. The Fos-LacZ breeding line of rats (Wistar-TG[Fos-LacZ]1Ottc) was generously provided by Drs. Nobo Suto and Friedbert Weiss (The Scripps Research Institute, La Jolla, CA) to Dr. Perrine by material transfer agreement.

References

[1] A. Villringer, U. Dirnagl, Coupling of brain activity and cerebral blood flow: basis of functional neuroimaging, Cereb. Brain Metab. Rev. 7 (3) (1995) 240–276.
[2] G.H. Glover, Overview of functional magnetic resonance imaging, Neurosurg. Clin. North Am. 22 (2) (2011) 133-vii.
[3] S. Gottschalk, O. Degtyaruk, B. Mc Larney, J. Rebling, M.A. Hutter, X.L. Deán-Ben, S. Shoham, D. Razansky, Rapid volumetric optoacoustic imaging of neural dynamics across the mouse brain, Nat. Biomed. Eng. 3 (5) (2019) 392–401.
[4] J. Kang, H.K. Zhang, S.D. Kadam, J. Fedorko, H. Valentine, A.P. Malla, P. Yan, M. M. Harraz, J.U. Kang, A. Rahmim, A. Gjedde, L.M. Loew, D.F. Wong, E.M. Boctor, Transcranial recording of electrophysiological neural activity in the rodent brain in vivo using functional photoacoustic imaging of near-infrared voltage-sensitive dye, Front. Neurosci. 13 (579) (2019).
[5] F. Cruz, E. Koya, D. Guez-Barber, J. Bossert, C. Lupica, Y. Shaham, B. Hope, New technologies for examining the role of neuronal ensembles in drug addiction and fear, 2013.
[6] F.C. Cruz, F. Javier Rubio, B.T. Hope, Using c-fos to study neuronal ensembles in corticostriatal circuitry of addiction, Brain Res. 2015 (1628) 157–173.
[7] R. Quintana-Feliciano, C. Gobin, L. Kane, B. Sortman, S. Rakela, A. Genovese, B. Tunstall, D. Caprioli, S.D. Iñiguez, B.L. Warren, Food-seeking behavior is mediated by Fos-expressing neuronal ensembles formed at first learning in rats, eNeuro 8 (2) (2021). ENEURO.0373-20.2021.
[8] A. Grosso, G. Santoni, E. Manassero, A. Renna, B. Sacchetti, A neuronal basis for fear discrimination in the lateral amygdala, Nat. Commun. 9 (1) (2018) 1214.
[9] E. Knapska, S. Maren, Reciprocal patterns of c-Fos expression in the medial prefrontal cortex and amygdala after extinction and renewal of conditioned fear, Learn Mem. 16 (8) (2009) 486–493.
[10] K. Gulmez Karaca, J. Kupke, D.V.C. Brito, B. Zeuch, C. Thome, D. Weichenhan, P. Lutsik, C. Plass, A.M.M. Oliveira, Neuronal ensemble-specific DNA methylation strengthens engram stability, Nat. Commun. 11 (1) (2020) 639.
[11] O. Khalaf, S. Resch, L. Dixsaut, V. Gorden, L. Glauser, J. Gräff, Reactivation of recall-induced neurons contributes to remote fear memory attenuation, Science 360 (6394) (2018) 1239–1242.
[12] L.R. Whitaker, B.L. Warren, M. Venniro, T.C. Harte, K.B. McPherson, J. Beidel, J. M. Bossert, Y. Shaham, A. Bonci, B.T. Hope, Bidirectional modulation of intrinsic excitability in rat prelimbic cortex neuronal ensembles and non-ensembles after operant learning, J. Neurosci. 37 (36) (2017) 8845–8856.
[13] L. Kane, M. Venniro, R. Quintana-Feliciano, R. Madangopal, F.J. Rubio, J. M. Bossert, D. Caprioli, Y. Shaham, B.T. Hope, B.L. Warren, Fos-expressing neuronal ensemble in rat ventromedial prefrontal cortex encodes cocaine seeking but not food seeking in rats, Addict. Biol. 26 (3) (2021), e12943.
[14] S. Cole, S.E. Keefer, L.C. Anderson, G.D. Petrovich, Medial prefrontal cortex neural plasticity, orexin receptor 1 signaling, and connectivity with the lateral hypothalamus are necessary in cue-potentiated feeding, J. Neurosci. 40 (8) (2020) 1744–1755.
[15] L.S. Brebner, J.J. Ziminski, G. Margetts-Smith, M.C. Sieburg, H.M. Reeve, T. Nowotny, J. Hirrlinger, T.G. Heintz, L. Lagnado, S. Kato, K. Kobayashi, L. A. Ramsey, C.N. Hall, H.S. Crombag, E. Koya, The emergence of a stable neuronal ensemble from a wider pool of activated neurons in the dorsal medial prefrontal cortex during appetitive learning in mice, J. Neurosci. 40 (2) (2020) 395–410.
[16] B.L. Warren, L. Kane, M. Venniro, P. Selvam, R. Quintana-Feliciano, M.P. Mendoza, R. Madangopal, L. Komer, L.R. Whitaker, F.J. Rubio, J.M. Bossert, D. Caprioli, Y. Shaham, B.T. Hope, Separate vmPFC ensembles control cocaine self-administration versus extinction in rats, J. Neurosci. 39 (37) (2019) 7394–7407.
[17] A. Laque, G.L. De Ness, G.E. Wagner, H. Nedelescu, A. Carroll, D. Watry, T.M. Kerr, E. Koya, B.T. Hope, F. Weiss, G.I. Elmer, N. Suto, Anti-relapse neurons in the infralimbic cortex of rats drive relapse-suppression by drug omission cues, Nat. Commun. 10 (1) (2019) 3934.
[18] Y.-X. Xue, Y.-Y. Chen, L.-B. Zhang, L.-Q. Zhang, G.-D. Huang, S.-C. Sun, J.-H. Deng, Y.-X. Luo, Y.-P. Bao, P. Wu, Y. Han, B.T. Hope, Y. Shaham, J. Shi, L. Lu, Selective inhibition of amygdala neuronal ensembles encoding nicotine-associated memories inhibits nicotine preference and relapse, Biol. Psychiatry 82 (11) (2017) 781–793.
[19] E. Koya, G. Margetts-Smith, B.T. Hope, Daun02 INactivation of Behaviorally Activated Fos-expressing Neuronal Ensembles, Curr. Protoc. Neurosci. 76 (2016) 8 36 1–8 36 17.
[20] G. de Guglielmo, E. Crawford, S. Kim, L.F. Vendruscolo, B.T. Hope, M. Brennan, M. Cole, G.F. Koob, O. George, Recruitment of a neuronal ensemble in the central nucleus of the amygdala is required for alcohol dependence, J. Neurosci. 36 (36) (2016) 9446–9453.
[21] S. Pfarr, M.W. Meinhardt, M.L. Klee, A.C. Hansson, V. Vengeliene, K. Schönig, D. Bartsch, B.T. Hope, R. Spanagel, W.H. Sommer, Losing control: excessive alcohol seeking after selective inactivation of cue-responsive neurons in the infralimbic cortex, J. Neurosci. 35 (30) (2015) 10750.
[22] E. Koya, S.A. Golden, B.K. Harvey, D.H. Guez, A. Berkow, D.E. Simmons, J. M. Bossert, S.G. Nair, J.L. Uejima, M.T. Marin, T. Mitchell, D. Farquhar, S. Ghosh, B.J. Mattson, B.T. Hope, Targeted disruption of cocaine-activated accumbens neurons prevents context-specific sensitization, Nat. Neurosci. 12 (8) (2009) 1069–1073.
[23] K. Kratkiewicz, R. Manwar, Y. Zhou, M. Mozaffarzadeh, K. Avanaki, Technical considerations in the Verasonics research ultrasound platform for developing a photoacoustic imaging system, Biomed. Opt. Express 12 (2) (2021) 1050–1084.
[24] J.I. Matchynski, R. Manwar, K.J. Kratkiewicz, R. Madangopal, V.A. Lennon, K. M. Makki, A.L. Reppen, A.R. Woznicki, B.T. Hope, S.A. Perrine, A.C. Conti, K. Avanaki, Direct measurement of neuronal ensemble activity using photoacoustic imaging in the stimulated Fos-LacZ transgenic rat brain: a proof-of-principle study, Photoacoustics 24 (2021), 100297.
[25] T.H. Kim, M.J. Schnitzer, Fluorescence imaging of large-scale neural ensemble dynamics, Cell 185 (1) (2022) 9–41.
[26] M.B. VanElzakker, M.K. Dahlgren, F.C. Davis, S. Dubois, L.M. Shin, From Pavlov to PTSD: The extinction of conditioned fear in rodents, humans, and in anxiety disorders, Neurobiol. Learn. Mem. 113 (2014) 3–18.
[27] M.A. Smith, S. Banerjee, P.W. Gold, J. Glowa, Induction of c-fos mRNA in rat brain by conditioned and unconditioned stressors, Brain Res. 578 (1) (1992) 135–141.
[28] C.H. Beck, H.C. Fibiger, Conditioned fear-induced changes in behavior and in the expression of the immediate early gene c-fos: with and without diazepam pretreatment, J. Neurosci. 15 (1 Pt 2) (1995) 709–720.
[29] A.A. Shah, D. Treit, Excitotoxic lesions of the medial prefrontal cortex attenuate fear responses in the elevated-plus maze, social interaction and shock probe burying tests, Brain Res. 969 (1–2) (2003) 183–194.
[30] I. Vidal-Gonzalez, B. Vidal-Gonzalez, S.L. Rauch, G.J. Quirk, Microstimulation reveals opposing influences of prelimbic and infralimbic cortex on the expression of conditioned fear, Learn. Mem. 13 (6) (2006) 728–733.
[31] A. Burgos-Robles, I. Vidal-Gonzalez, E. Santini, G.J. Quirk, Consolidation of fear extinction requires NMDA receptor-dependent bursting in the ventromedial prefrontal cortex, Neuron 53 (6) (2007) 871–880.
[32] A. Burgos-Robles, I. Vidal-Gonzalez, G.J. Quirk, Sustained conditioned responses in prelimbic prefrontal neurons are correlated with fear expression and extinction failure, J. Neurosci.: Off. J. Soc. Neurosci. 29 (26) (2009) 8474–8482.
[33] S.C. Kim, Y.S. Jo, I.H. Kim, H. Kim, J.-S. Choi, Lack of medial prefrontal cortex activation underlies the immediate extinction deficit, J. Neurosci. 30 (3) (2010) 832–837.
[34] V. Laurent, R.F. Westbrook, Inactivation of the infralimbic but not the prelimbic cortex impairs consolidation and retrieval of fear extinction, Learn. Mem. 16 (9) (2009) 520–529.
[35] M.R. Milad, G.J. Quirk, Fear extinction as a model for translational neuroscience: ten years of progress, Annu. Rev. Psychol. 63 (1) (2012) 129–151.
[36] C.-h Chang, J.D. Berke, S. Maren, Single-unit activity in the medial prefrontal cortex during immediate and delayed extinction of fear in rats, PLOS ONE 5 (8) (2010), e11971.
[37] D. Sierra-Mercado, N. Padilla-Coreano, G.J. Quirk, Dissociable roles of prelimbic and infralimbic cortices, ventral hippocampus, and basolateral amygdala in the expression and extinction of conditioned fear, Neuropsychopharmacology 36 (2) (2011) 529–538.
[38] J.H. Cho, S.D. Rendall, J.M. Gray, Brain-wide maps of Fos expression during fear learning and recall, Learn Mem. 24 (4) (2017) 169–181.
[39] I.M. James, M. Rayyan, J.K. Karl, M. Rajtarun, A.L. Veronica, M.M. Kassem, T. H. Bruce, C.C. Alana, A.P. Shane, A. Kamran, Photoacoustic imaging of fear conditioning neuronal ensembles using a Fos-LacZ gene reporter system in the rat brain in vivo after intrathecal X-gal injection, Proc. SPIE (2021).
[40] C.P. Allen, K. Park, A. Li, N.D. Volkow, G.F. Koob, Y. Pan, X.-T. Hu, C. Du, Enhanced neuronal and blunted hemodynamic reactivity to cocaine in the prefrontal cortex following extended cocaine access: optical imaging study in anesthetized rats, Addict. Biol. 24 (3) (2019) 485–497.
[41] N.R. Council. Guide for the Care and Use of Laboratory Animals, Eighth ed., The National Academies Press, Washington, DC, 2011.
[42] A.K. Dutta, S. Santra, A. Harutyunyan, B. Das, M.J. Lisieski, L. Xu, T. Antonio, M.E. A. Reith, S.A. Perrine, D-578, an orally active triple monoamine reuptake inhibitor,

displays antidepressant and anti-PTSD like effects in rats, Eur. J. Pharm. 862 (2019), 172632.
[43] D. Au, Y.Au Li, Y.Au Li, Z.Au Tian, Y.Au Xu, Guo, Direct intrathecal injection of recombinant adeno-associated viruses in adult mice, JoVE 144 (2019), e58565.
[44] C. Au, C.Au Njoo, R.Au Heinl, Kuner, In Vivo SiRNA transfection and gene knockdown in spinal cord via rapid noninvasive lumbar intrathecal injections in mice, JoVE 85 (2014), e51229.
[45] C. Mestre, T. Pélissier, J. Fialip, G. Wilcox, A. Eschalier, A method to perform direct transcutaneous intrathecal injection in rats, J. Pharmacol. Toxicol. Methods 32 (4) (1994) 197–200.
[46] J. Morgan, D. Cohen, J. Hempstead, T. Curran, Mapping patterns of c-fos expression in the central nervous system after seizure, Science 237 (4811) (1987) 192–197.
[47] M. Mozaffarzadeh, A. Mahloojifar, M. Orooji, K. Kratkiewicz, S. Adabi, M. Nasiriavanaki, Linear-array photoacoustic imaging using minimum variance-based delay multiply and sum adaptive beamforming algorithm, J. Biomed. Opt. 23 (2) (2018), 026002.
[48] M. Mozaffarzadeh, A. Mahloojifar, M. Orooji, S. Adabi, M. Nasiriavanaki, Double-stage delay multiply and sum beamforming algorithm: application to linear-array photoacoustic imaging, IEEE Trans. Biomed. Eng. 65 (1) (2018) 31–42.
[49] R. Manwar, L. Saint-Martin, K. Avanaki, Couplants in acoustic biosensing systems, Chemosensors 10 (5) (2022) 181.
[50] N.C. Burton, M. Patel, S. Morscher, W.H. Driessen, J. Claussen, N. Beziere, T. Jetzfellner, A. Taruttis, D. Razansky, B. Bednar, V. Ntziachristos, Multispectral opto-acoustic tomography (MSOT) of the brain and glioblastoma characterization, Neuroimage 65 (2013) 522–528.
[51] J. Yanai, Strain and sex differences in the rat brain, Acta Anat. 103 (1979) 150–158.
[52] G. Paxinos. The rat brain in stereotaxic coordinates / George Paxinos, Charles Watson, 7th ed., Academic Press, Sydney, 2013.
[53] J. Schindelin, I. Arganda-Carreras, E. Frise, V. Kaynig, M. Longair, T. Pietzsch, S. Preibisch, C. Rueden, S. Saalfeld, B. Schmid, J.-Y. Tinevez, D.J. White, V. Hartenstein, K. Eliceiri, P. Tomancak, A. Cardona, Fiji: an open-source platform for biological-image analysis, Nat. Methods 9 (2012) 676.
[54] Y. Benjamini, Y. Hochberg, Controlling the false discovery rate: a practical and powerful approach to multiple testing, J. R. Stat. Soc.: Ser. B (Methodol.) 57 (1) (1995) 289–300.
[55] R.J. Handa, K.M. Nunley, M.R. Bollnow, Induction of c-fos mRNA in the brain and anterior pituitary gland by a novel environment, Neuroreport 4 (9) (1993) 1079–1082.
[56] A. Yochiy, L.R.G. Britto, M.H.L. Hunziker, Novelty, but not operant aversive learning, enhances Fos and Egr-1 expression in the medial prefrontal cortex and hippocampal areas of rats, Behav. Neurosci. 126 (6) (2012) 826–834.
[57] A. Badiani, M.M. Oates, H.E.W. Day, S.J. Watson, H. Akil, T.E. Robinson, Amphetamine-induced behavior, dopamine release, and c-fos mRNA expression: modulation by environmental novelty, J. Neurosci. 18 (24) (1998) 10579–10593.
[58] G.M. Kasof, R.J. Smeyne, T. Curran, J.I. Morgan, Developmental expression of Fos-lacZ in the brains of postnatal transgenic rats, Dev. Brain Res. 93 (1) (1996) 191–197.
[59] A. Pajser, C. Foster, B. Gaeddert, C.L. Pickens, Extended operant training increases infralimbic and prelimbic cortex Fos regardless of fear conditioning experience, Behav. Brain Res. 414 (2021), 113476.
[60] V.Y. Cao, Y. Ye, S. Mastwal, M. Ren, M. Coon, Q. Liu, R.M. Costa, K.H. Wang, Motor learning consolidates arc-expressing neuronal ensembles in secondary motor cortex, Neuron 86 (6) (2015) 1385–1392.
[61] C.H. Liu, Y.R. Kim, J.Q. Ren, F. Eichler, B.R. Rosen, P.K. Liu, Imaging cerebral gene transcripts in live animals, J. Neurosci. 27 (3) (2007) 713–722.
[62] R. Cao, J. Zhao, L. Li, L. Du, Y. Zhang, Y. Luo, L. Jiang, S. Davis, Q. Zhou, A. de la Zerda, L.V. Wang, Optical-resolution photoacoustic microscopy with a needle-shaped beam, Nat. Photonics 17 (1) (2023) 89–95.
[63] R. Bi, Q. Ma, H. Mo, M. Olivo, Y. Pu, 8 - Optical-Resolution Photoacoustic Microscopy of Brain Vascular Imaging in Small Animal Tumor Model Using Nanosecond Solid-State Laser, in: R.R. Alfano, L. Shi (Eds.), Neurophotonics and Biomedical Spectroscopy, Elsevier, 2019, pp. 159–187.

James I. Matchynski graduated with high distinction receiving a B.S. with a dual major in Chemistry and Biochemistry from the University of Michigan Dearborn in 2015. He is now pursuing a dual MD/PhD degree at Wayne State University School of Medicine with the PhD in translational neuroscience. His area of research includes using behavioral models of fear-learning to find mechanisms behind posttraumatic stress disorder (PTSD) and developing a functional imaging technique that uses photoacoustic and transgenic technology to track changes in Fos neuronal ensembles within rats *in vivo*.

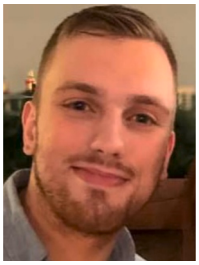

Timothy Cilley received his BS at Michigan State University in 2020. He currently works as a research assistant with the Conti Laboratory and the NueroCAST Laboratory at Wayne State University. The majority of his research is comprised of image analysis and applying behavioral models of fear-learning to find mechanisms behind Post-Traumatic Stress Disorder (PTSD) and other related anxiety disorders.

Nareen Sadik received her bachelor's degree from Wayne State University in 2019. She has a Bachelor of Science in Nutrition and Food Science. She is currently working as a clinical research coordinator in the department of Psychiatry and Behavioral Neurosciences at Wayne State University. Her research interests include post-traumatic stress disorder and substance use.

Kassem Makki received his BA from Wayne State University, Detroit, Michigan in 2017. His bachelor's is in Biological Sciences In 2021 he graduated from Michigan State College of Osteopathic Medicine. He completed his Transitional Year Residency at St. Mary Mercy Livonia Hospital in June of 2022 and is currently a first year Emergency Medicine Resident at New York Presbyterian Brooklyn Methodist Hospital. His research interests include pediatric emergency medicine, medical malpractice, and quality improvement. He aspires to participate in translationally relevant research throughout his professional career and pursue a fellowship in Pediatric Emergency Medicine.

Min Wu received her BA from Shaanxi Normal University, Xi'an China in 1990. She is currently a senior research associate in the Conti Laboratory at the John D. Dingell VA Medical Center in Detroit, MI. There her work is focused on investigating the interactions between experimental traumatic brain injury or traumatic stress and abused substances, such as alcohol and opioids. She specializes in cell culture, immunolabeling, and microscopy.

Rayyan Manwar received his PhD from the University of Windsor, Windsor, Ontario in 2017. His bachelor's is in Electrical and Electronic Engineering from the Islamic University of Technology (IUT), Gazipur, Bangladesh in 2011. Currently, he is a post-doctoral fellow at OPIRA Lab, Wayne State University, Detroit, MI. His research interests include MEMS-based design, fabrication, and characterization, and photoacoustic and ultrasound imaging.

Alexander Woznicki received his BS in Psychology from Wayne State University and is currently a second-year medical student at Oakland University William Beaumont school of Medicine. His area of research includes investigation of the interaction between opioids and traumatic brain injury in the generation of oxidative stress. He is interested in continued study regarding the neurological response to physical trauma.

Srinivasu Kallakuri earned his doctorate in Anatomy and Cell Biology (Neurosciences) from Wayne State University (Detroit, MI) in 2010. He is currently a Research Scientist in the Department of Psychiatry and Behavioral Neurosciences. His research interest includes the effects of repeated trauma (TBI or stress), drug-taking behavior, and the role of inflammation. Prior to this, he worked in the Department of Biomedical Engineering and was involved in numerous studies related to blunt and blast traumatic brain injury.

Cynthia L. Arfken received her PhD in Chronic Disease Epidemiology from Yale University and completed a post-doctoral fellowship in alcohol research at the University of California, Berkeley. She is a Professor of Psychiatry and Behavioral Neurosciences at Wayne State University School of Medicine in Detroit, Michigan. In addition to providing biostatistical assistance to research and clinical colleagues, she has directed her own research on substance use disorders and has served on numerous NIH, FDA, and SAMHSA review panels. To facilitate putting research into practice, she is the Vice Chair of the Substance Use Disorder Oversight Policy Board for the largest county in Michigan.

Bruce Hope received his PhD in Neurological Research from the University of British Columbia in 1991. He is currently Chief of the Neuronal Ensembles in the Addiction Section at the Intramural Research Program of the National Institute on Drug Abuse (NIDA IRP). He is examining how neuronal ensembles encode memories underlying maladaptive drug-seeking behaviors and relapse and developing novel tools for studying persistent molecular and cellular engrams within these ensembles that maintain these long-term memories.

Mohammad R.N. Avanaki. He is currently an Associate Professor of Biomedical Engineering Department at the University of Illinois in Chicago. Prior to this position, he was an Associate Professor of Biomedical Engineering Department at Wayne State University. He received his Ph.D. degree from the University of Kent, the United Kingdom with an Outstanding Achievement Honor in Medical Optical Imaging and Computing in 2012. His areas of expertise are design and development of photoacoustic imaging technology and optical coherence tomography for biomedical applications to solve critical problems in brain and skin imaging.

Alana Conti Alana Conti received her PhD in Neuroscience from the University of Pennsylvania in 2003. She is currently a Professor of Psychiatry and Behavioral Neurosciences at Wayne State University School of Medicine and a Health Science Specialist at the John D. Dingell VA Medical Center in Detroit, MI. She investigates the interactions between experimental traumatic brain injury or traumatic stress and abused substances, such as alcohol and opioids. Specifically, she aims to identify the mechanisms by which trauma increases susceptibility to pain, leading to drug and alcohol misuse and how drug exposure impacts trauma recovery.

Shane A. Perrine earned his doctorate in Biomedical Sciences from Kent State University (Kent, OH, USA) in 2002. Dr. Perrine conducted postdoctoral fellowships at the Center for Substance Abuse Research at Temple University (Philadelphia, PA, USA) and the Brain Imaging Research Division at Wayne State University (Detroit, MI, USA). He is currently an Associate Professor of Psychiatry and Behavioral Neurosciences at Wayne State University School of Medicine. Dr. Perrine's preclinical laboratory focuses on brain and behavioral relationships that underlie substance abuse and posttraumatic stress.